JOURNAL OF COMPUTATIONAL PHYSICS 109, 1–15 (1993)

Cell Vertex Algorithms for the Compressible Navier–Stokes Equations

P. I. CRUMPTON, J. A. MACKENZIE, AND K. W. MORTON

Oxford University Computing Laboratory, Numerical Analysis Group, 11 Keble Road, Oxford OX1 3QD, England

Received August 11, 1992

Finite volume methods on a structured quadrilateral or hexahedral mesh have very attractive properties for the first-order Euler equations, with the cell vertex scheme being preferred for its accuracy and greater compactness. Somewhat surprisingly, although this scheme is less compact than its competitors for the second-order convection-diffusion or Navier–Stokes equations, its accuracy properties are even more remarkable, being attained with no upwinding parameters. However, there are difficulties in setting up and solving an appropriate set of cell residual equations. In this paper we present a consistent cell vertex discretisation, together with multigrid pseudo-time stepping procedures which come close to setting the cell residuals to zero; the generalised Lax–Wendroff procedure that is used is a significant difference from previous attempts to use similar schemes. Results are given for laminar flow, where careful comparisons are made to demonstrate accuracy, and turbulent flow with an algebraic turbulence model.

1. INTRODUCTION

Throughout the last decade there has been intense discussion over the relative merits of various cell centre and cell vertex formulations of the finite volume methods which are widely used for computing compressible flows. We present the case here for a specific cell vertex formulation for the Navier–Stokes equations. In the scheme the discrete equations are set up on a structured body-fitted mesh which is quadrilateral in two dimensions and hexahedral in three dimensions. The mesh is generated within a multiblock framework, with multigrid to be applied over the whole structure. The discrete equation solver used is a pseudo-time stepping algorithm which is based on the Lax–Wendroff scheme first used by Ni [24] and developed in [9, 18, 21, 19, 4].

For a system of first-order equations on a rectangular mesh, the cell vertex method reduces to the well-known box scheme associated with the names of many different authors working in different application areas—Thomas, Keller, and Preissman, for example—and is widely valued for its compactness, accuracy, and unconditional stability. Similarly, for the steady Euler equations its properties have been widely appreciated and studied, both in one dimension [2, 13, 23] and in two dimensions [24, 9, 21]. These include maintenance of accuracy under mesh distortion, absence of all but the chequer-board spurious error mode, and availability of shock recovery and similar techniques for treating shocks with only the minimal amount of artificial viscosity.

The distinctive feature of the cell vertex discretisation is that conservation is applied to the body-fitted mesh cells, or primary cells, with the unknowns held at the cell vertices and on the boundaries—see Fig. 1. By contrast, we use the term cell centre for schemes in which conservation is applied to these primary cells but the unknowns are associated with the cell centres, and therefore are not on the boundaries, such as in [11]. Another class of schemes are the vertex-based or vertex-centred methods where the unknowns are held at the primary cell vertices but conservation is applied over a secondary system of cells centred on the unknowns, with a half cell being used at the boundary, such as in [5, 10].

We are firmly of the view that in a Navier–Stokes discretisation the inviscid and viscous fluxes should be consistently approximated over the same cell edges/faces of the mesh, in order to ensure a proper flux balance at convergence. However, although vertex-based schemes of this type have been studied in [10], we are aware of no other authors who have developed this approach with the cell vertex scheme as just defined; it is advocated in [8, 12] for the one-dimensional convection-diffusion equation and Burgers' equation respectively; and in [6, 26] it is considered for the Navier–Stokes equations but is rejected, apparently because of difficulties in solving the equations. Several authors, see, e.g., [16, 27, 6], have instead combined a cell vertex approach to the inviscid fluxes with a cell centre approach to the viscous terms.

The main reason for not using the consistent cell vertex formulation lies in the difficulty in setting up and solving the discrete equation system. As a first demonstration of this problem, consider the one-dimensional hyperbolic problem $\mathbf{f}_x(\mathbf{w}) = \mathbf{s}(\mathbf{w}, x)$ for the unknown $\mathbf{w}$, to be approximated at

0021-9991/93 $5.00

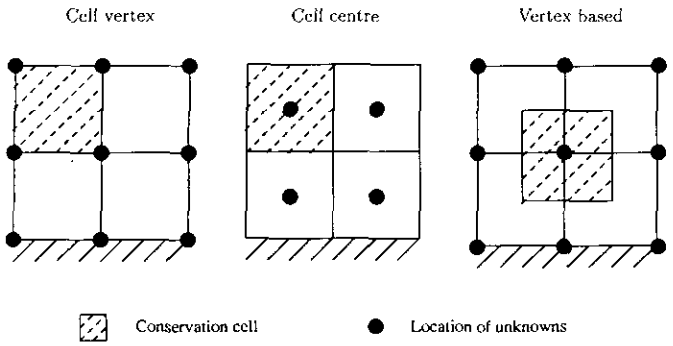

FIG. 1. Conservation cells and unknowns for various finite volume methods.

mesh points x_j by $\mathbf{W}_j$. The cell vertex discretisation yields the cell equations

$$\mathbf{F}_j - \mathbf{F}_{j-1} = \tfrac{1}{2}(x_j - x_{j-1})(\mathbf{S}_j + \mathbf{S}_{j-1}), \tag{1.1}$$

where $\mathbf{F}_j := \mathbf{f}(\mathbf{W}_j)$ and $\mathbf{S}_j := \mathbf{s}(\mathbf{W}_j, x_j)$. Suppose first that all the eigenvalues of the flux Jacobian matrix $\mathbf{A} := \partial \mathbf{f}/\partial \mathbf{w}$ are positive. Then all the boundary data is given on the left, at x_0 say, and the application of (1.1) for $j = 1, 2, ..., J$ successively determines all values $\{\mathbf{W}_j\}_{j=1}^{J}$ by the solution of a local nonlinear system. This can be achieved quickly and the resulting solution values are second-order accurate on any non-uniform grid. This is the ideal situation for the cell vertex method. However, more generally, as for a transonic nozzle flow problem, the eigenvalues have different signs which change over the domain. Some boundary data will be given on the right and some on the left, and the total number of equations given by (1.1) may not match the number of unknowns. However, the discrete problem can be made to count correctly if in setting up the equations due account is taken of cells over which the eigenvalues change sign; for the nozzle problem this entails splitting a residual at the sonic point and combining two at the shock. A highly accurate solution is then obtained by solving the discrete equations, which can be achieved by an efficient procedure described in [23]. A closely related scheme has been used by Casier *et al.* [2], and the use of such switches at sonic and shock points is, of course, well established.

Next, consider the cell vertex discretisation of the one-dimensional scalar convection-diffusion equation $(-\varepsilon w_x + f)_x = s(x)$, with $f \equiv f(w)$, i.e.,

$$\begin{aligned}(-\varepsilon W'_j + F_j) - (-\varepsilon W'_{j-1} + F_{j-1}) \\ = \tfrac{1}{2}(x_j - x_{j-1})(S_j + S_{j-1}),\end{aligned} \tag{1.2}$$

where $F_j := f(W_j)$ and an approximation of the gradient is introduced of the form

$$W'_j := [\alpha_j D_+ + (1 - \alpha_j) D_-]\, W_j. \tag{1.3}$$

Here D_+ and D_- are the forward and backward divided difference operators, respectively, and α_j is a weighting parameter such as $\alpha_j = (x_{j+1} - x_j)/(x_{j+1} - x_{j-1})$. The result is a four-point scheme based on the interval (x_{j-1}, x_j), whereas virtually all other schemes that have been devised for such problems are three-point schemes centred at a node x_j, where a standard second-order difference is used for the diffusion and some sort of upwinded difference is needed for the convection term. However, for the cell vertex method with Dirichlet data prescribing $w(x)$ at each end of the interval, there will be $J-1$ unknowns and J intervals so that (1.2) cannot be satisfied on all of them. The solution adopted in [15, 7] is to associate each unknown with the cell on its upwind side; so if $a \equiv \partial f/\partial w > 0$ everywhere and hence any boundary layer is on the right, the right-hand cell is ignored and (1.2) is solved for $j = 1, ..., J-1$, with extrapolation for W'_0 used to replace (1.3). A detailed analysis in [15, 7] shows that this four-point approximation has remarkable monotonicity and accuracy properties on virtually any mesh and for any value of ε. For a three-point scheme these properties can generally only be obtained with careful adjustment of an upwind parameter.

Unfortunately, we have not yet been able to devise procedures for the multidimensional Navier–Stokes equations which correspond to the careful association of cell residual equations with nodal unknowns described in the two examples given above. Our use of a Lax–Wendroff procedure constitutes a compromise which will often somewhat degrade the quality of the solution; but the use of the generalised Lax–Wendroff scheme introduced in [19, 4] greatly reduces the damage. Suppose, for example, we denote by $\Delta_{j-1/2}$ the difference between the left- and the right-hand sides of (1.2); then a Lax–Wendroff iteration can be written

$$\begin{aligned}W_j^{n+1} = W_j^n - \frac{\nu_N}{2a_j^n}[(1 + \nu_C)\,\Delta_{j-1/2}^n + (1 - \nu_C)\,\Delta_{j+1/2}^n], \\ j = 1, 2, ..., J-1,\end{aligned} \tag{1.4}$$

where ν_N and ν_C are CFL parameters, and at convergence the quantity in square brackets is set to zero. With a standard Lax–Wendroff scheme $\nu_N = \nu_C = \nu$ and convergence requires choosing $\nu < 1$. This means that, in general, the system of equations actually solved depends on the choice of this iteration parameter; the individual cell residuals decouple only when there is no boundary condition on the right, as in the nondissipative case $\varepsilon = 0$, and a one-sided update at $j = J$ sets $\Delta_{J-1/2} = 0$. At the worst extreme $\nu \to 0$, corresponding to a simple averaging of the residuals which might be used in a Runge–Kutta update, the properties of the cell vertex scheme are entirely destroyed; and any choice $\nu < 1$ will clearly lead to oscillating residuals. The first advantage of the generalised Lax–Wendroff procedure, then, is to separate the choice of ν_C, which determines the equations solved at convergence, from that of ν_N which

defines the iteration. Convergence requires $v_C v_N < 1$; but the second advantage is that this allows the choice $v_C > 1$, which leads to a monotone decay of the residuals like $(v_C - 1)/(v_C + 1)$. In particular, taking $v_C = 1$ corresponds to full upwinding and has the desired effect of setting $\Delta_{j-1/2} = 0$ for $j = 1, ..., J-1$. Note that taking v_C too large could give too thick a boundary layer because of added diffusion, so that care is needed with systems of equations—see [23] for a discussion of a similar situation with shocks.

It is this use of the generalised Lax–Wendroff update that distinguishes the present method from previous attempts to use the cell vertex scheme for the Navier–Stokes equations.

The development of these ideas to solve the Navier–Stokes equations is set out in the rest of the paper as follows. The discretisation of the inviscid and viscous fluxes is described in the next section, and Section 3 is devoted to describing the pseudo-time stepping procedures used. Finally, in Section 4, results are presented and discussed for various aerofoils at low Reynolds numbers, using the laminar equations, and at higher Reynolds numbers, using an algebraic turbulence model.

2. DISCRETISATION OF INVISCID AND VISCOUS FLUXES

In this section we describe the cell vertex discretisation of a system of steady two-dimensional, viscous conservation laws of the form

$$\mathbf{f}_x(\mathbf{w}, \nabla\mathbf{w}) + \mathbf{g}_y(\mathbf{w}, \nabla\mathbf{w}) = 0, \qquad (x, y) \in \Omega. \tag{2.1}$$

Here $\mathbf{w}(x, y)$ is a vector of unknowns and $\mathbf{f}(\mathbf{w}, \nabla\mathbf{w})$ and $\mathbf{g}(\mathbf{w}, \nabla\mathbf{w})$ are vector-valued flux functions which can be split into inviscid and viscous components, which are often treated differently, such that

$$\mathbf{f}(\mathbf{w}, \nabla\mathbf{w}) = \mathbf{f}^I(\mathbf{w}) + \mathbf{f}^V(\mathbf{w}, \nabla\mathbf{w})$$

and

$$\mathbf{g}(\mathbf{w}, \nabla\mathbf{w}) = \mathbf{g}^I(\mathbf{w}) + \mathbf{g}^V(\mathbf{w}, \nabla\mathbf{w}). \tag{2.2}$$

In the case of the Navier–Stokes equations the unknowns and the fluxes have the nondimensionalised form

$$\mathbf{w} = \begin{pmatrix} \rho \\ \rho u \\ \rho v \\ \rho E \end{pmatrix}, \quad \mathbf{f}^I = \begin{pmatrix} \rho u \\ \rho u^2 + p \\ \rho uv \\ \rho uH \end{pmatrix}, \quad \mathbf{g}^I = \begin{pmatrix} \rho v \\ \rho uv \\ \rho v^2 + p \\ \rho vH \end{pmatrix} \tag{2.3}$$

$$\mathbf{f}^V = \begin{pmatrix} 0 \\ -\tau_{xx} \\ -\tau_{xy} \\ -u\tau_{xx} - v\tau_{xy} + q_x \end{pmatrix}, \quad \mathbf{g}^V = \begin{pmatrix} 0 \\ -\tau_{xy} \\ -\tau_{yy} \\ -u\tau_{xy} - v\tau_{yy} + q_y \end{pmatrix}, \tag{2.4}$$

where ρ, u, v, p, E, and H denote the density, the two Cartesian components of velocity, the pressure, the total specific energy, and the total specific enthalpy, respectively. The deviatoric stress and heat conduction terms are given by

$$\tau_{xx} = \frac{2\mu}{3\,\mathrm{Re}}\left(2\frac{\partial u}{\partial x} - \frac{\partial v}{\partial y}\right), \qquad \tau_{xy} = \frac{\mu}{\mathrm{Re}}\left(\frac{\partial u}{\partial y} + \frac{\partial v}{\partial x}\right),$$
$$\tau_{yy} = \frac{2\mu}{3\,\mathrm{Re}}\left(2\frac{\partial v}{\partial y} - \frac{\partial u}{\partial x}\right), \tag{2.5}$$

$$q_x = -\frac{\kappa}{(\gamma - 1)\,M_\infty^2\,\mathrm{Re}\,\mathrm{Pr}}\frac{\partial T}{\partial x},$$
$$q_y = -\frac{\kappa}{(\gamma - 1)\,M_\infty^2\,\mathrm{Re}\,\mathrm{Pr}}\frac{\partial T}{\partial y}, \tag{2.6}$$

where γ, κ, Re, Pr, and M_∞ denote the adiabatic constant, the coefficient of thermal conductivity, the Reynolds number, the Prandtl number, and the freestream Mach number, respectively. The viscosity μ is assumed to vary with temperature according to Sutherland's law. For turbulent flows we have used only the zero equation model of Baldwin and Lomax [1], in which the Reynolds stresses and thermal fluxes are modelled by an effective turbulent viscosity and turbulent Prandtl number.

The domain Ω in (2.1) is assumed to be an open, connected subset of $\mathbb{R}^2$ with a locally Lipschitz boundary $\partial\Omega$ on which appropriate boundary conditions are specified. Since our main interest is in external flows, Ω should be infinite; but for computational purposes it is truncated and appropriate far-field boundary conditions introduced—see Section 3.3. We also assume that a steady solution $\mathbf{w}(x, y)$ to this problem exists and satisfies an integrated form of (2.1), namely

$$\oint_{\partial\tilde{\Omega}} (\mathbf{f}\,dy - \mathbf{g}\,dx) = \mathbf{0} \qquad \forall\tilde{\Omega} \subset \Omega, \tag{2.7}$$

where $\tilde{\Omega}$ is any sub-region of Ω.

We suppose that Ω is partitioned by a set of nonoverlapping, convex quadrilateral cells Ω_α, i.e., $\bar{\Omega} = \bigcup_\alpha \bar{\Omega}_\alpha$. The finite volume discretisation of (2.7) is then based on approximating the boundary integral for each Ω_α by an appropriate quadrature rule. For the cell vertex method this is the trapezoidal rule and leads to the definition of numerical flux functions $\mathbf{F}$ and $\mathbf{G}$, computed from the cell vertex approximation $\mathbf{W}$, and a set of cell residuals

$$\mathbf{R}_\alpha(\mathbf{W}) := \frac{1}{V_\alpha}\oint_{\partial\Omega_\alpha} (\mathbf{F}\,dy - \mathbf{G}\,dx) \qquad \forall\Omega_\alpha, \tag{2.8}$$

where V_α is the measure of Ω_α. With this scaling, $\mathbf{R}_\alpha(\mathbf{W})$

represents the rate of change of the average of $\mathbf{W}$ in Ω_α for the unsteady problem; for the steady problem the aim is obviously to try to drive these residuals to zero. Moreover, $\mathbf{R}_\alpha(\mathbf{w})$, evaluated with exact solution $\mathbf{w}$, corresponds to the truncation error of the cell vertex discretisation of (2.1).

2.1. *Integration of the Fluxes*

To integrate the fluxes along each cell edge we suppose that $\mathbf{W}$, $\mathbf{F}$, and $\mathbf{G}$ all have the same functional representation over each cell. This is given by the bilinear mapping in (ξ, η) which takes the canonical square $(\xi, \eta) \in [-1, 1] \times [-1, 1]$ into Ω_α (Fig. 2) and uses the coordinates of the cell vertices—see Appendix A. From this form for $\mathbf{W}$ we can recover values of $\nabla\mathbf{W}$ at each vertex and hence construct $\mathbf{F}(\mathbf{W}, \nabla\mathbf{W})$ and $\mathbf{G}(\mathbf{W}, \nabla\mathbf{W})$ of the same form. Then to calculate $\mathbf{R}_\alpha(\mathbf{W})$ we have

$$\oint_{\partial\Omega_\alpha} (\mathbf{F}\,dy - \mathbf{G}\,dx) = \tfrac{1}{2}[(\mathbf{F}_1 - \mathbf{F}_3)\,\delta y_{24} + (\mathbf{F}_2 - \mathbf{F}_4)\,\delta y_{31} - (\mathbf{G}_1 - \mathbf{G}_3)\,\delta x_{24} - (\mathbf{G}_2 - \mathbf{G}_4)\,\delta x_{31}], \tag{2.9}$$

where $\delta x_{ij} = x_i - x_j$ and similarly for δy_{ij}.

For the Euler equations, this compact four-point approximation has many favourable characteristics, the most important being its accuracy on distorted grids. Morton and Paisley [21] have shown that the truncation error is second-order accurate as long as the cells are parallelograms to within $O(h)$, where h is the diameter of the cell, i.e., the orientations of opposite sides differ by $O(h)$; and second-order accuracy of the global error has been established for two-dimensional scalar advection by Süli [28] assuming similar regularity of the computational mesh.

Recovery of $\nabla\mathbf{W}$ for the calculation of the viscous fluxes is most easily carried out by using a divergence form and Gauss' theorem again. Thus for a point (x_0, y_0) near the centre of a sub-region $\tilde{\Omega}$, we have

$$\mathbf{W}_{x|(x_0, y_0)} \approx \frac{1}{V_{\tilde{\Omega}}} \int_{\tilde{\Omega}} \nabla \cdot (\mathbf{W}, \mathbf{0})\, d\Omega = \frac{1}{V_{\tilde{\Omega}}} \oint_{\partial\tilde{\Omega}} \mathbf{W}\, dy. \tag{2.10}$$

The most direct application of the idea is to each vertex of the mesh, using diagonals of the surrounding cells to define $\tilde{\Omega}$, as shown schematically in Fig. 3a, and the trapezoidal rule. If $\mathbf{x}_1$ is a vertex in a regular structured mesh at which four quadrilaterals meet so that $\tilde{\Omega}$ is the quadrilateral $NWSE$, we have the formulae

$$(\mathbf{W}_x)_1 = \frac{1}{2V_{NWSE}}[(\mathbf{W}_E - \mathbf{W}_W)\,\delta y_{NS} + (\mathbf{W}_N - \mathbf{W}_S)\,\delta y_{WE}], \tag{2.11a}$$

$$(\mathbf{W}_y)_1 = -\frac{1}{2V_{NWSE}}[(\mathbf{W}_E - \mathbf{W}_W)\,\delta x_{NS} + (\mathbf{W}_N - \mathbf{W}_S)\,\delta x_{WE}]. \tag{2.11b}$$

Unfortunately, this approximation is second-order accurate only on a smoothly varying mesh; we need the quadrilateral $NWSE$ to be within $O(h)$ of a parallelogram, as well as the previous assumption on the primary cells. However, the approach has the advantage of simplicity and can easily be generalised to cases where more than four quadrilaterals meet at one node, as will be the case with multiblock meshes. In Appendix A it is shown how (2.11) can be derived from $\nabla\mathbf{W}$ in each cell, evaluated at the vertex; it may be possible to derive more accurate formulae from this approach but this has not yet been pursued.

A more accurate approach, in general, is the following: first, the average gradient in each of the primary cells is obtained by integrating $\nabla \cdot (\mathbf{W}, \mathbf{0})$ and $\nabla \cdot (\mathbf{0}, \mathbf{W})$ over each cell as shown above. As long as the primary cells are parallelograms to within $O(h)$ these averages are second-order approximations to the gradient at the centroids of the cells. In Appendix A it is shown that this procedure is equivalent to calculating the gradient at the centroid of the

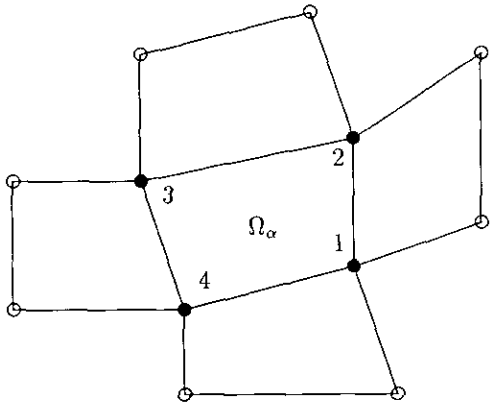

FIG. 2. Mesh values to calculate $\mathbf{R}_\alpha$; ● inviscid, ● and ○ viscous flow.

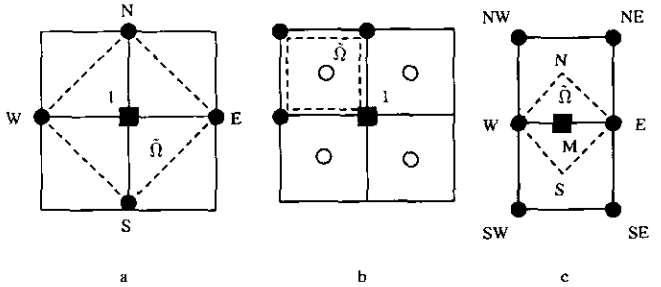

FIG. 3. Three techniques of gradient recovery: (a) directly at vertex 1; (b) through centroid values and interpolation; (c) an edge approximation for WE.

primary cell directly from the assumed isoparametric bilinear variation of $\mathbf{W}$ within each cell. The gradient at the primary cell vertices can then be recovered by passing a bilinear interpolant through the centroid values and evaluating it at the primary cell vertices, as indicated in Fig. 3b.

Finally, it may sometimes be appropriate to calculate directly the average of $\nabla \mathbf{W}$ along an edge. A simple edge approximation of this kind is obtained by integrating $\nabla \cdot (\mathbf{W}, \mathbf{0})$ and $\nabla \cdot (\mathbf{0}, \mathbf{W})$ over the quadrilateral formed by the end points of the edge and the centroids of two cells, as indicated in Fig. 3c; in doing so one sets $W_N = (W_{NW} + W_{NE} + W_W + W_E)/4$ and $W_S = (W_{SW} + W_{SE} + W_W + W_E)/4$. Other cell edge approximations may be formed with greater accuracy properties but they are likely to be computationally more expensive.

There remains the problem of recovering $\nabla \mathbf{W}$ on a boundary, principally on a solid wall boundary as we have used inviscid far-field boundary conditions. Moreover, only normal derivatives are needed: for the temperature these are given by an assumed insulating wall condition; and for the velocity, the technique of Fig. 3a, when applied to that part of the quadrilateral in the domain, gives a first-order accurate condition. Second-order accuracy is achieved by extrapolation from this value and that at the first interior vertex.

3. SOLUTION PROCEDURE

Having established the definition of a cell-based residual $\mathbf{R}_\alpha$ based on (2.8), it remains to describe the solution procedure to determine $\mathbf{W}$. Difficulties associated with solving the system of cell-based equations $\mathbf{R}_\alpha = \mathbf{0}\ \forall \Omega_\alpha \subset \Omega$ include:

- the counting of equations and unknowns, and the associated problem of imposing appropriate boundary conditions;
- the equation deficiency across sonic lines and inaccuracies across shocks;
- the chequer-board error mode.

As mentioned in the Introduction, the counting difficulty arises through the possible disparity between the number of cell-based equations and boundary conditions, and the number of unknowns. This problem, and the closely related one of shocks and sonic lines, has been studied and overcome in a number of special cases—see [15, 23]. To circumvent this issue here, however, we shall adopt the procedure of setting combinations of cell residuals to zero, by using a generalised Lax–Wendroff scheme to distribute contributions from each cell residual to its four corners; this produces a "node-based" equation for each unknown which with boundary conditions will always count correctly. The objective is to carry out this distribution process so that when the node-based equations are solved the cell residuals are also driven close to zero.

Fourier analysis of the linearised cell residual, as in [19, 22], shows the presence of a spurious chequer-board mode, which is only controlled by the boundary conditions. In external flow problems this control is too weak and therefore some fourth-order artificial dissipation terms are needed to avoid slow convergence and residual errors. There are other spurious modes which arise when the flow is parallel to the mesh and these have to be similarly controlled. We shall show below that these added terms have negligible effect on the converged solution while significantly affecting the convergence rate.

3.1. *Lax–Wendroff Distribution Matrices*

The cell-based residuals $\mathbf{R}_\alpha$ are mapped onto the four vertices of each cell by means of distribution matrices $D_{\alpha,j}$, to form a system of node-based equations of the form

$$\mathbf{N}_j(\mathbf{W}) := \frac{\sum_{\alpha=1}^{p} V_\alpha D_{\alpha,j} \mathbf{R}_\alpha}{\sum_{\alpha=1}^{p} V_\alpha} = \mathbf{0}, \tag{3.1}$$

where p is the number of cells meeting at node j and normally $p = 4$. Many alternative schemes are available for choosing these distribution matrices and then constructing an iterative procedure to solve the system (3.1), together with appropriate boundary conditions—see [23] for a comparison of schemes in one dimension. We here use a relatively simple generalised Lax–Wendroff pseudo-time stepping procedure.

For a cell Ω_α, as in Fig. 4, the distribution matrices $D_{\alpha,j}$ are defined by

$$D_{\alpha,1} := I - \nu_C \frac{\Delta t_\alpha}{V_\alpha} (\delta y_{42} A_\alpha - \delta x_{42} B_\alpha) \tag{3.2a}$$

$$D_{\alpha,2} := I - \nu_C \frac{\Delta t_\alpha}{V_\alpha} (\delta y_{13} A_\alpha - \delta x_{13} B_\alpha) \tag{3.2b}$$

$$D_{\alpha,3} := I - \nu_C \frac{\Delta t_\alpha}{V_\alpha} (\delta y_{24} A_\alpha - \delta x_{24} B_\alpha) \tag{3.2c}$$

$$D_{\alpha,4} := I - \nu_C \frac{\Delta t_\alpha}{V_\alpha} (\delta y_{31} A_\alpha - \delta x_{31} B_\alpha), \tag{3.2d}$$

where ν_C is a global CFL number associated with the second-order update, Δt_α is a maximal cell-based local time step, and A_α and B_α are the Jacobians of the inviscid fluxes evaluated at the cell centre. We set

$$\Delta t_\alpha = \min(\Delta t_\alpha^I, \Delta t_\alpha^V), \tag{3.3a}$$

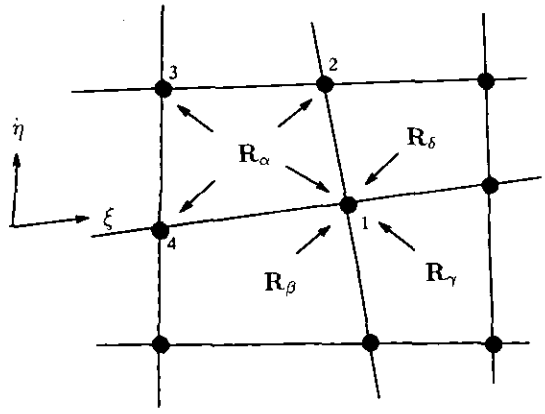

FIG. 4. Distribution of the cell residual $\mathbf{R}_\alpha$ to the four cell vertices and of the four cell residuals to the update at the vertex 1.

where Δt_α^I and Δt_α^V are the inviscid and viscous time steps defined by

$$\Delta t_\alpha^I = \frac{V_\alpha}{\sqrt{(|u|+c)^2 \max((\delta y_{42})^2, (\delta y_{13})^2) + (|v|+c)^2 \max((\delta x_{42})^2, (\delta x_{13})^2)}} \quad (3.3b)$$

and

$$\Delta t_\alpha^V = \frac{V_\alpha^2}{2\varepsilon(\max((\delta y_{42})^2, (\delta y_{13})^2) + \max((\delta x_{42})^2, (\delta x_{13})^2))}. \quad (3.3c)$$

Here u, v, and c are averaged at the cell centre, and ε is the maximum eigenvalue of the linearised Navier–Stokes terms [14]; that is,

$$\varepsilon = \frac{1}{\rho\,\mathrm{Re}} \max\left(\frac{4\mu}{3}, \frac{\kappa\gamma}{\mathrm{Pr}}\right). \quad (3.4)$$

These are generalisations of the time steps derived from a Fourier stability analysis in [19, 14]—see Appendix B for a detailed derivation and extension of the results in [19, 14].

The total update at an interior vertex of a structured mesh block involves four cells and 21 nodal values; referring to Fig. 4, it has the form

$$\mathbf{W}_1^{n+1} = \mathbf{W}_1^n - \omega_1 \frac{\left(\begin{array}{c} V_\alpha D_{\alpha,1}^n \mathbf{R}_\alpha^n + V_\beta D_{\beta,1}^n \mathbf{R}_\beta^n + V_\gamma D_{\gamma,1}^n \mathbf{R}_\gamma^n \\ + V_\delta D_{\delta,1}^n \mathbf{R}_\delta^n \end{array}\right)}{V_\alpha + V_\beta + V_\gamma + V_\delta}, \quad (3.5)$$

where

$$\omega_1 = \nu_N \Delta t_1 = \nu_N \min(\Delta t_\alpha, \Delta t_\beta, \Delta t_\gamma, \Delta t_\delta)$$

and ν_N is a global node-based CFL number.

The form of the distribution matrices in (3.2) is derived in [18] from a Taylor–Galerkin approximation to the unsteady problem. The introduction of both a cell-based and a node-based time-step and CFL number was advocated in [19] (but the notation used here has been modified to make for simpler programming), because they play different roles. Only $\nu_C \Delta t_\alpha$ affects the quality of the converged approximation; while $\nu_N \Delta t_1$ is the main control over the convergence of the iteration. For example, it is shown in [23] for one-dimensional inviscid flows that the node-based ν_N controls the phase speed of waves and hence the transport of errors to the boundary, while taking the cell-based ν_C greater than ν_N gives some second-order damping, rather than the usual fourth-order obtained with $\nu_C = \nu_N$; more importantly, taking $\nu_C \geqslant 1$ helps in the objective of setting to zero the cell residuals, rather then merely the nodal residuals.

A Fourier analysis is given in Appendix B for the two scalar problems $w_t + aw_x + bw_y = 0$ and $w_t + aw_x - \varepsilon w_{xx} = 0$. This, first, justifies the convergence conditions

$$\nu_N \leqslant \nu_C, \qquad \nu_N \nu_C < 1 \quad (3.6)$$

that we use for inviscid flows; as seen in (B.20), the x- and y-components of ν_C and ν_N must have the same ratio, and although by (B.26) and Fig. 12, some relaxation of the standard condition $\nu_x^2 + \nu_y^2 < 1$ is possible when $\nu_C > \nu_N$, we shall not use it. Second, the introduction of viscous terms makes little difference to these conditions, as shown by the analysis of the convection-diffusion problem. As is well known, if a conventional Lax–Wendroff method for the convection equation has added to it a central difference approximation to a diffusion terms εw_{xx}, then the stability condition $\nu^2 \leqslant 1$ has to be strengthened to $\nu^2 + 2\varepsilon \Delta t/(\Delta x)^2 \leqslant 1$. For our scheme, in the usual case $\nu_C^2 \geqslant \frac{1}{2}$,(3.6) is merely strengthened by $2\nu_C^2 \varepsilon \Delta t/(\Delta x)^2 \leqslant 1$, corresponding to (3.3c) when $\nu_C = 1$; see Fig. 11 for a comparison. This is an unexpected advantage of our consistent approach to the approximation of the inviscid and viscous fluxes and is important not only for the viscous fluxes but also in taking account of artificial viscosity terms. It means that in practice the time-steps given by (3.3a) are seldom affected by the viscous terms except in a very thin boundary layer.

3.2. *Dissipation Terms*

The extent to which we need to use dissipation terms is one measure of the further development needed with the cell vertex method. The second- and fourth-order dissipation terms used here are an adaptation from the cell centre approach of [11] and are used to control oscillations due to shocks and due to spurious modes such as the chequer-board, respectively. All coefficients are cell-based and multiply differences along cell edges. We use the notation δ_ξ^2 and

δ_η^2 to denote second differences along the body-fitted coordinate lines, and for the coordinate direction ξ define

$$\tau_\alpha^{(2,\xi)} := \frac{\varepsilon^{(2)}}{\Delta t_\alpha} \max_{j \in \Omega_\alpha} \{\kappa_j^\xi\} \tag{3.7a}$$

$$\tau_\alpha^{(4,\xi)} := \max\left\{0, \frac{\varepsilon^{(4)}}{\Delta t_\alpha} - \tau_\alpha^{(2,\xi)}\right\}, \tag{3.7b}$$

where

$$\kappa_j^\xi = \frac{|\delta_\xi^2 p_j|}{(4+\delta_\xi^2) p_j}, \tag{3.7c}$$

with similar quantities for the η coordinate direction. These are the forms used in laminar flow problems, but for turbulent flow both $\varepsilon^{(2)}$ and $\varepsilon^{(4)}$ are scaled by the factor $\min\{1, M/M_\infty\}$. Using the notation of Fig. 4, the artificial viscosity vector for cell Ω_α and node 1 is then given by

$$\begin{aligned} A_{\alpha,1}(\mathbf{W}) := {} & \tau_\alpha^{(2,\xi)}(\mathbf{W}_1 - \mathbf{W}_4) + \tau_\alpha^{(2,\eta)}(\mathbf{W}_1 - \mathbf{W}_2) \\ & - \tau_\alpha^{(4,\xi)}(\delta_\xi^2 \mathbf{W}_1 - \delta_\xi^2 \mathbf{W}_4) - \tau_\alpha^{(4,\eta)}(\delta_\eta^2 \mathbf{W}_1 - \delta_\eta^2 \mathbf{W}_2). \end{aligned} \tag{3.8}$$

These terms are combined with the cell-based residual terms in formulae (3.1) and (3.5) through the replacement

$$D_{\alpha,j}\mathbf{R}_\alpha \to D_{\alpha,j}\mathbf{R}_\alpha + \mathbf{A}_{\alpha,j}. \tag{3.9}$$

It is an important feature of these definitions that when the $\mathbf{A}_{\alpha,j}$ of Eq. (3.8) are summed over the vertices of cell Ω_α there is complete internal cancellation. Hence by (3.2), (3.9) sums to $4\mathbf{R}_\alpha$, which ensures that at convergence, even if all the individual cell residuals are not zero, at least we satisfy a global conservation principle. Note that at domain (and also at inter-block) boundaries the second differences which involve exterior points are set to zero; numerical experiments with dummy inter-block boundaries show that this makes very little difference to convergence rates or final solutions.

These are very unsophisticated artificial viscosity terms, being scalar in character and using the very simple switching based on (3.7). It may seem strange that we use undivided differences, so that a linear variation on a non-smooth mesh contributes to the second difference. This was prompted by the observation that the chequer-board mode, which is our main target, is independent of the mesh geometry; experiments with divided differences have not shown significant improvements.

3.3. *Boundary Conditions*

For solid wall boundaries the no-slip condition $\mathbf{q} = (u, v) = \mathbf{0}$ is implemented directly by overwriting the Lax–Wendroff update, obtained with dummy exterior cells which have zero residuals but non-zero measures. If the wall temperature were specified then this would be dealt with in the same way; otherwise, an insulated wall condition is incorporated in the flux calculation as already described.

In the absence of well-established energy absorbing boundary conditions for general external Navier–Stokes calculations, we have used far-field conditions based on the Euler equations. As at a solid boundary, a predicted state $\mathbf{W}^{n+*}$ is obtained from the boundary-modified Lax–Wendroff update. This is then combined with a state at infinity $\mathbf{W}_\infty$ which takes account of the circulation around the body as in [31]. Confining ourselves to subsonic flow at infinity, at inflow points the Riemann variables $R^\pm := \mathbf{q}\cdot\mathbf{n} \pm 2c/(\gamma-1)$, corresponding to the outward normal $\mathbf{n}$ are calculated, R^+ from $\mathbf{W}^{n+*}$ and R^- from $\mathbf{W}_\infty$, and combined to give $(\mathbf{q}\cdot\mathbf{n})^{n+1}$ and c^{n+1} at the point; the tangential velocity and the entropy are also taken from $\mathbf{W}_\infty$ to complete the calculation of $\mathbf{W}^{n+1}$. At outflow points, it is the pressure that is taken from $\mathbf{W}_\infty$ and combined with the outgoing Riemann variable, tangential velocity, and entropy from $\mathbf{W}^{n+*}$ to give $\mathbf{W}^{n+1}$.

The extent of the compromises that we have made in implementing the cell vertex method should now be clear, and some of the consequences will be seen in the numerical results of the next section. We have not attempted to set up and solve a system of equations corresponding to setting to zero the selected components of selected or modified cells residuals, as we can with simpler problems. We have, instead, used some of the flexibility provided by the generalised Lax–Wendroff scheme to define a set of nodal residuals which, apart from the effects of the artificial viscosity terms, can be set to zero and which we hope will lead to driving most of the cell residuals to zero.

4. NUMERICAL RESULTS

In this section the results are presented for two external aerodynamics problems to demonstrate the accuracy of the consistent cell vertex discretisation. We have used a single block C-mesh with the vertex-based discretisation of the viscous fluxes given by (2.11). A multigrid acceleration procedure based on the standard full approximation scheme (FAS) has been applied to the Lax–Wendroff update, and typically gives a sixfold increase in the convergence rate. If the nodal equations (3.1) on a mesh h are written $\mathbf{N}_h(\mathbf{W}_h) = \mathbf{f}_h$ and R_h^H is the restriction operator from a fine to a coarse mesh, for the next coarser mesh we set

$$\mathbf{f}_H = R_h^H[\mathbf{f}_h - \mathbf{N}_h(\mathbf{W}_h)] + \mathbf{N}_H(R_h^H \mathbf{W}_h), \tag{4.1}$$

with $\mathbf{f}_h = \mathbf{0}$ on the finest mesh. Thus at each level the discrete problem is of the same form; but the second-order artificial

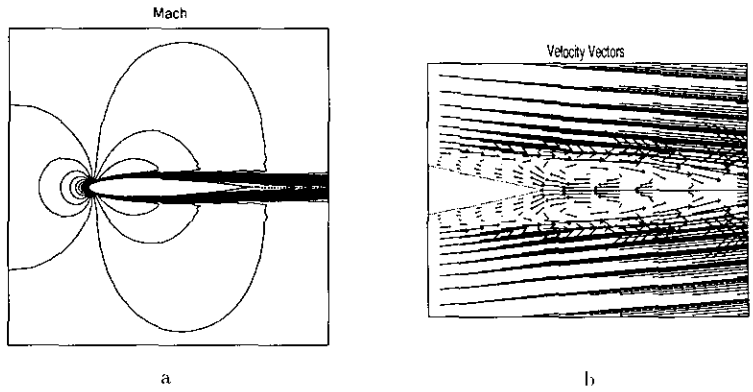

FIG. 5. NACA0012 aerofoil with $M_\infty = 0.5$, Re = 5000, $\alpha = 0°$: (a) Mach contours; (b) velocity vectors at the trailing edge.

dissipation is increased on the coarser meshes to cope with the smaller number of points in the boundary layer. The code has been fully vectorised in Fortran 77 for a Cray YMP supercomputer.

Our first problem is a well-documented laminar test case for subsonic flow over a NACA0012 aerofoil at zero angle of attack with Re = 5000 and $M_\infty = 0.5$. The mesh used has (193×49) nodes, with the far-field 20 chords from the aerofoil and the first mesh interval normal to the body of the order 10^{-4} chord lengths. The main feature of the solution is a recirculation region near the trailing edge of the aerofoil, see Fig. 5b. The separation point can be identified in Fig. 6b as that point where the skin friction coefficient becomes zero. More details of the calculations can be found in [20].

To demonstrate the minimal dependence of the cell vertex solution on the fourth-order artificial viscosity parameter $\varepsilon^{(4)}$, the viscous and inviscid drag parameters, C_D^V and C_D^I, and the separation point are given in Table I for calculations with a wide range of $\varepsilon^{(4)}$, and $\varepsilon^{(2)}$ set to zero. Clearly, a 16-fold change of $\varepsilon^{(4)}$ essentially affects only the work required to reduce the nodal residuals to a given tolerance, a work unit being defined as a calculation of the fine grid residual. Table II shows good agreement with other results in the literature, given the relatively coarse mesh.

Figure 7 shows the tangential velocity and corresponding budget plots for the nodal and cell residuals, across the boundary layer at 10% and 75% of the chord. It is clear that, for the value of $\varepsilon^{(4)} = 0.01$ taken here, artificial viscosity plays a minor rôle in the nodal residual balance, although its effect at the edge of the boundary layer has increased significantly by the 75% point. Moreover, the right-hand plots show that for this problem we have come close to achieving the target of setting the cell residuals to zero; note that artificial viscosity terms are not included here and that the lack of cell residual balance is some measure of its deleterious effects.

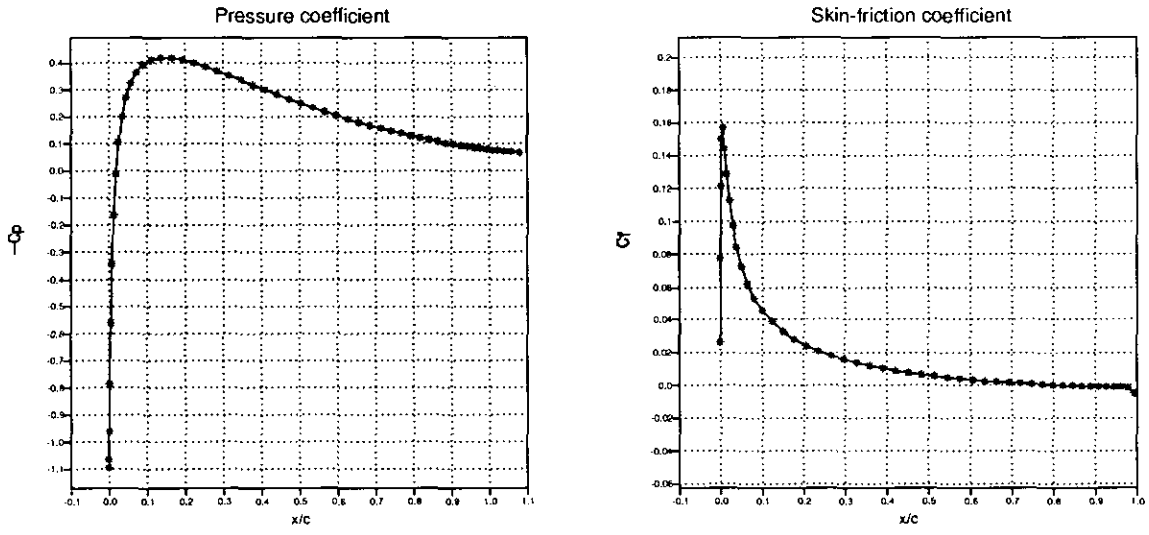

FIG. 6. NACA0012 aerofoil with $M_\infty = 0.5$, Re = 5000, $\alpha = 0°$: (a) pressure coefficient; (b) local skin-friction coefficient.

TABLE I

Variation of Viscous and Inviscid Drag Coefficients, Separation Point, and Computational Work with the Coefficient of Fourth-Order Artificial Dissipation, for NACA0012 Aerofoil with $M_\infty = 0.5$, $\mathrm{Re} = 5000$, and $\alpha = 0°$

$\varepsilon^{(4)}$	C_D^I	C_D^V	Separation point percentage of chord	Work units
0.0005	0.0226	0.0325	81.9	8329
0.002	0.0226	0.0325	82.0	7648
0.008	0.0226	0.0326	82.1	6593
0.032	0.0226	0.0330	82.3	5298

TABLE II

Comparison with Other Authors for NACA0012 Aerofoil with $M_\infty = 0.5$, $\mathrm{Re} = 5000$, and $\alpha = 0°$

Author	Grid	C_D^I	C_D^V	Separation point percentage of chord
Present	193×49	0.0226	0.0325	81.9
[17]	320×64	0.0229	0.0332	81.4
[16]	320×64	0.0219	0.0337	81.9

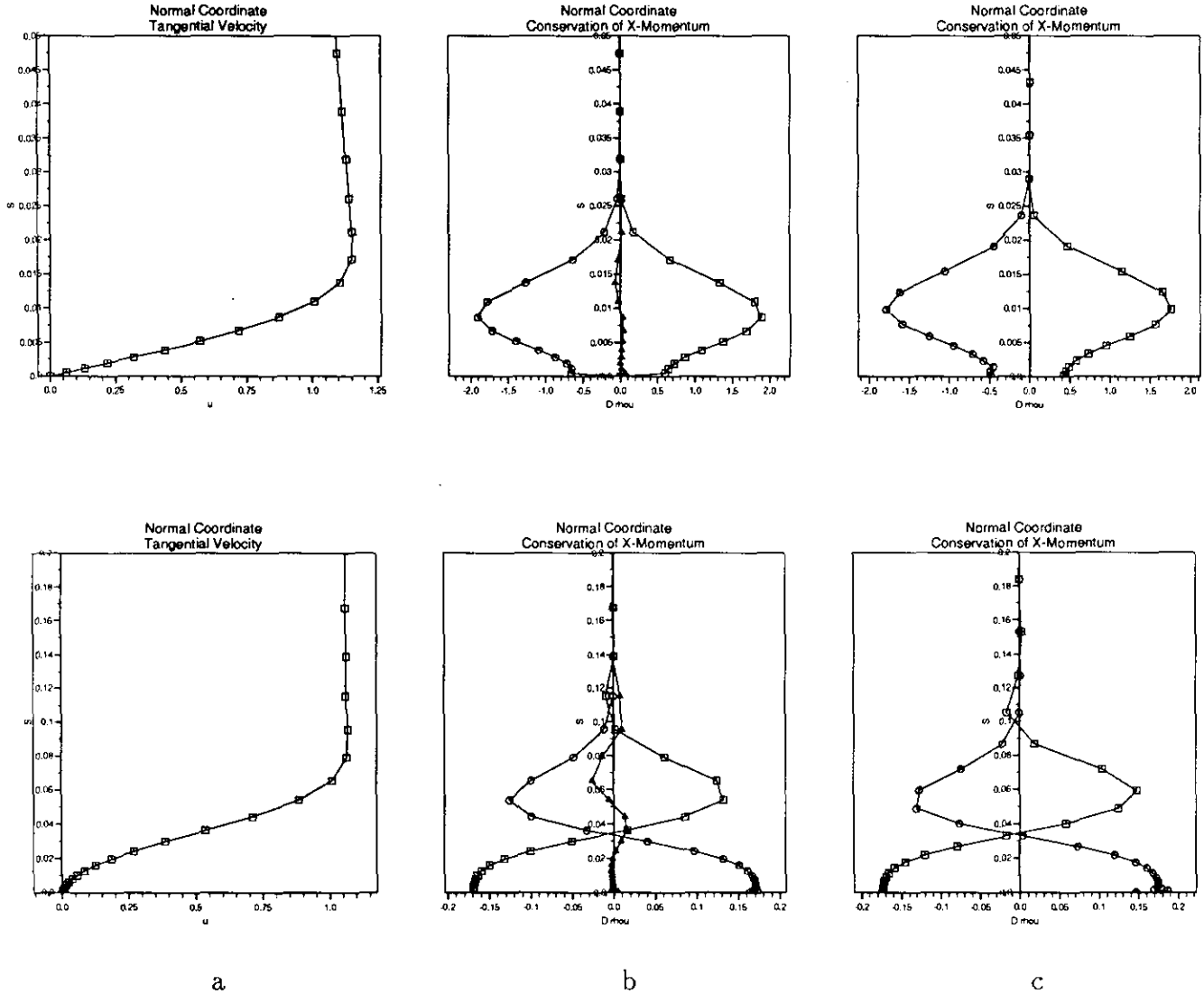

FIG. 7. Solution detail normal to NACA0012 at 10% chord (top) and at 75% chord (bottom): (a) tangential velocity. (b) nodal equation budget: □, inviscid; ⊕, viscous; △, artificial dissipation. (c) cell residual equation budget: □, inviscid; ⊕, viscous.

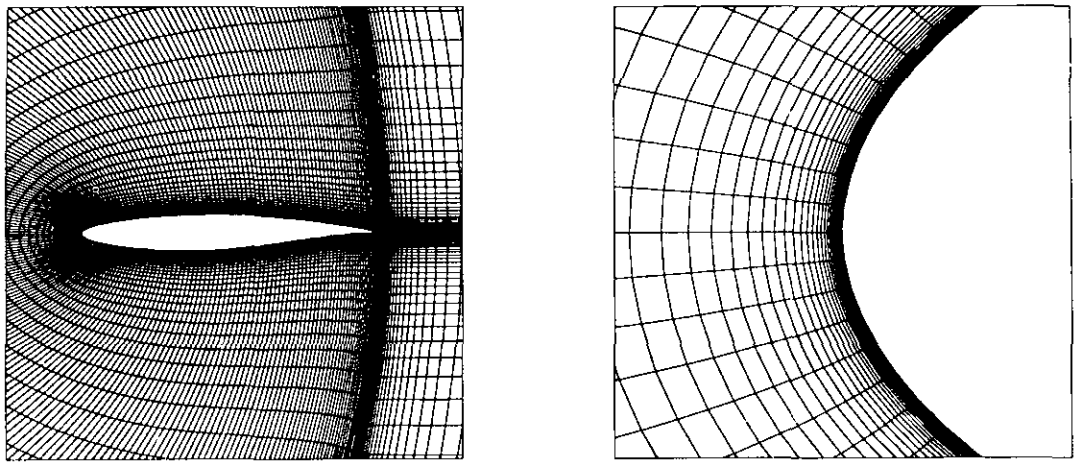

FIG. 8. RAE2822 aerofoil, with part of (289 × 81) grid.

The second problem considered is turbulent flow over an RAE 2822 aerofoil, Case 9 of Cook *et al.* [3], assumed to correspond to $\mathrm{Re} = 6.5 \times 10^6$, $M_\infty = 0.73$, and $\alpha = 2.79°$. The two-layer algebraic eddy viscosity model of [1] is used, with two modifications adopted from [27]—namely, use of the maximum local shear stress through the boundary layer and setting the constant $C_{WK} = 1.0$. Alternative surface definitions of the aerofoil have been used but results are presented here for that most commonly used by other authors. The mesh used is shown in Fig. 8; it has (289 × 81) nodes, with 225 on the aerofoil, the far-field situated 10 chord lengths from the aerofoil, and the first mesh interval normal to the body less than 10^{-5} of the chord length.

Comparison of the results with the experiment is shown in Fig. 9, and with other authors in Table III. There is close agreement with experiment on the pressure coefficient, and this can be improved by use of a camber-corrected aerofoil definition. The discrepancy in the skin-friction coefficient shown in Fig. 9 near the 60% chord length is thought to be due to the turbulence model and is in accord with the findings of other authors. In Fig. 10 we show budget plots for the residuals as in Fig. 7. They are clearly not as good in this case, although the extent to which the cell residuals are generally driven to zero is still very encouraging. The few oscillations very near the body require further investigation. The mesh has extremely high aspect ratios here, and near the leading edge this makes great demands on the recovery technique for $\nabla \mathbf{W}$; the form of the artificial viscosity and the switches incorporated in its definition are also rather crude. Attempts to exploit the flexibility in choosing $\nu_C > 1$ in the

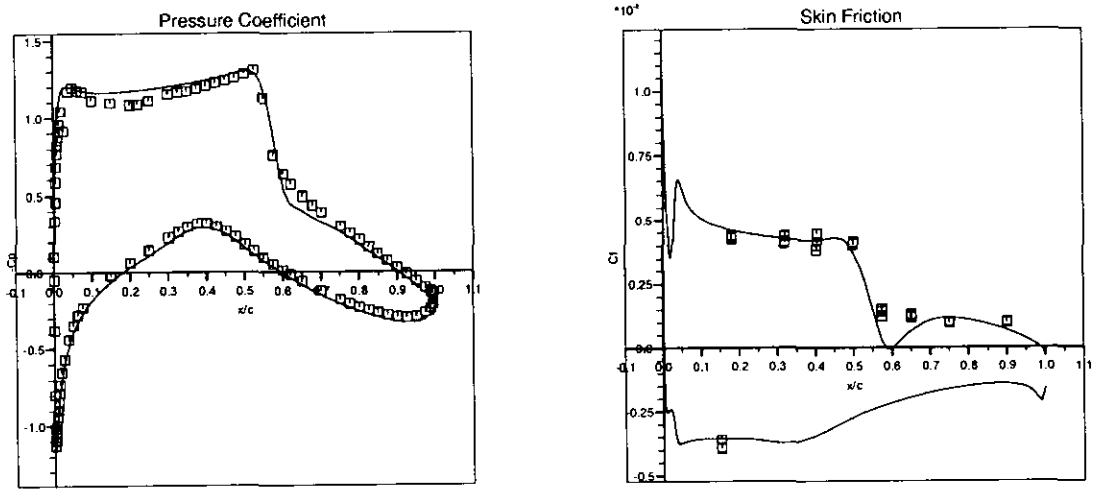

FIG. 9. RAE2822 aerofoil with $M_\infty = 0.73$, $\mathrm{Re} = 6.5 \times 10^6$, and $\alpha = 2.79°$: ———, cell vertex; □, experiment [3].

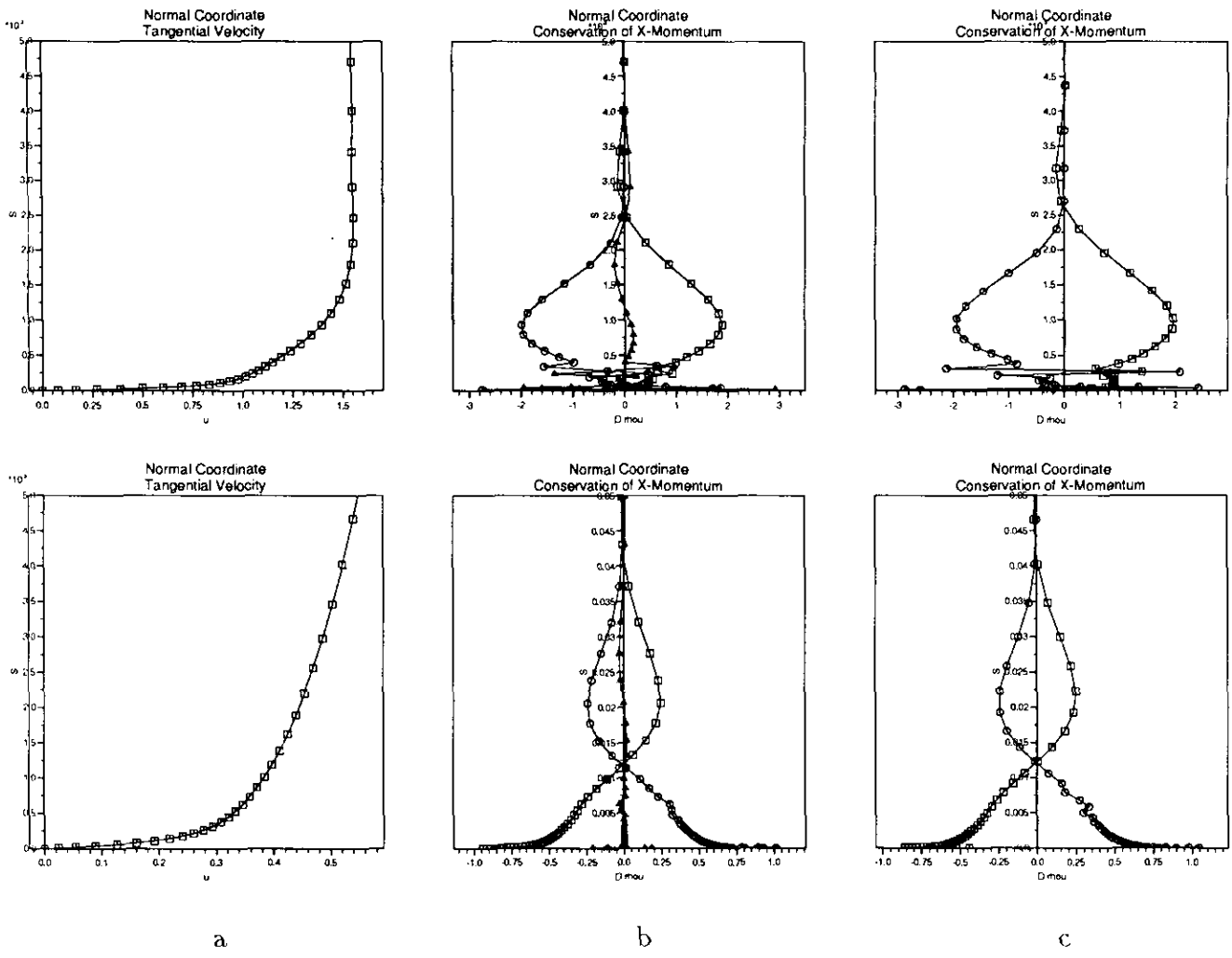

FIG. 10. Solution detail normal to RAE2822 at 10% chord (top) and at 90% chord (bottom): (a) tangential velocity. (b) nodal equation budget: □, inviscid; ⊕, viscous; △, artificial dissipation. (c) cell residual equation budget: □, inviscid; ⊕, viscous.

generalised Lax–Wendroff scheme show some effect, but this is limited by the use of a scalar ν_C (rather than the matrix-valued ν_C used in [23]) and the fact that only the inviscid Jacobians are used in (3.2), even in the boundary layer. Further developments to address these issues are in hand and will be reported in future publications.

TABLE III

Comparison with Other Authors for RAE2822 Aerofoil with $M_\infty = 0.73$, $\mathrm{Re} = 6.5 \times 10^6$, and $\alpha = 2.79°$

Author	Grid	C_L	C_D^I	C_D^V	C_D
Present	289 × 81	0.847	0.0122	0.0054	0.0176
[26]	257 × 65	0.842	0.0121	0.0055	0.0175
[29]	257 × 65	0.829	0.0124	0.0051	0.0175
[25]	249 × 51	0.824	0.0128	0.0050	0.0178
[30]	641 × 129	0.859	0.0124	0.0055	0.0179

5. CONCLUSIONS

The cell vertex finite volume methods described in this paper, in which the conservation cells correspond to the primary mesh cells and the unknowns are held at their vertices, differ radically from most other finite volume schemes. The advantage for high Reynolds number flows which contain large areas of essentially inviscid flow is the very compact stencil for the inviscid terms combined with the consistent treatment of viscous and inviscid fluxes.

The main disadvantage lies in the difficulty of setting up and solving the corresponding discrete equations. The procedure adopted here uses distribution matrices to form node-based equations which are solved using a standard relaxation procedure, accelerated with a multigrid technique. The distribution matrices are derived from a generalised Lax–Wendroff algorithm which goes a long way toward ensuring that the cell residuals are driven to zero at

convergence; and, with the consistent flux discretisation, its CFL convergence condition is barely affected by viscous effects.

Budget plots of the terms in the nodal residuals indicate the extent that artificial viscosity is needed to achieve a balance; but budget plots of the terms in the cell residuals, and their lack of balance, provide a much sharper check on accuracy and indeed are related to those used in a posteriori error estimates.

Results for laminar test problems show how well the objectives of the method are attained in practice; those for a turbulent problem are encouraging and indicate points which still need attention. However, the schemes given here are still quite simple, with scalar parameters used in defining both the distribution matrices and the artificial viscosity terms; many further developments are clearly possible which make use of decompositions based on the flux Jacobians, and these are in hand. Also the discretization, the analysis, and the test problems are all in two dimensions. A three-dimensional version of the code has been written but its testing is at an early stage.

APPENDIX A: CALCULATION OF GRADIENTS

Suppose local coordinates (ξ, η) are introduced such that the canonical square $[-1, 1] \times [-1, 1]$ is mapped onto the cell in Fig. 2 by the bilinear mapping

$$\mathbf{x}(\xi, \eta) = \sum_{i=1}^{4} \mathbf{x}_i \phi_i(\xi, \eta), \tag{A.1}$$

where

$$\begin{aligned} \phi_1(\xi, \eta) &= \tfrac{1}{4}(1+\xi)(1-\eta), \\ \phi_2(\xi, \eta) &= \tfrac{1}{4}(1+\xi)(1+\eta), \\ \phi_3(\xi, \eta) &= \tfrac{1}{4}(1-\xi)(1+\eta), \\ \phi_4(\xi, \eta) &= \tfrac{1}{4}(1-\xi)(1-\eta); \end{aligned} \tag{A.2}$$

and suppose that $W(\mathbf{x})$ has the same form in $\bar{\Omega}_\alpha$:

$$W(\mathbf{x}(\xi, \eta)) = \sum_{i=1}^{4} W_i \phi_i(\xi, \eta). \tag{A.3}$$

It is easy to calculate ∇W in terms of $\partial W/\partial \xi$ and $\partial W/\partial \eta$ from the relation

$$\begin{pmatrix} W_\xi \\ W_\eta \end{pmatrix} = J \begin{pmatrix} W_x \\ W_y \end{pmatrix} = \begin{pmatrix} x_\xi & y_\xi \\ x_\eta & y_\eta \end{pmatrix} \begin{pmatrix} W_x \\ W_y \end{pmatrix}, \tag{A.4}$$

where the Jacobian and (W_ξ, W_η) are

$$J = \frac{1}{4} \begin{pmatrix} (1-\eta)\,\delta x_{14} + (1+\eta)\,\delta x_{23} & (1-\eta)\,\delta y_{14} + (1+\eta)\,\delta y_{23} \\ (1+\xi)\,\delta x_{21} + (1-\xi)\,\delta x_{34} & (1+\xi)\,\delta y_{21} + (1-\xi)\,\delta y_{34} \end{pmatrix} \tag{A.5a}$$

$$(W_\xi, W_\eta) = \tfrac{1}{4}((1-\eta)\,\delta W_{14} + (1+\eta)\,\delta W_{23}, \; (1+\xi)\,\delta W_{21} + (1-\xi)\,\delta W_{34}). \tag{A.5b}$$

Putting $\xi = \eta = 0$ to obtain ∇W at the centroid, we have $\det J = V_\alpha/4$ and from (A.3) and (A.4) we have

$$W_{x|0,0} = \frac{1}{2V_\alpha} [(W_1 - W_3)\,\delta y_{24} + (W_2 - W_4)\,\delta y_{31}] \tag{A.6a}$$

$$W_{y|0,0} = -\frac{1}{2V_\alpha} [(W_1 - W_3)\,\delta x_{24} + (W_2 - W_4)\,\delta x_{31}], \tag{A.6b}$$

corresponding exactly to applying (2.10) to the primary cell Ω_α and hence comparable with (2.9). Similarly, putting $\xi = 1$, $\eta = -1$ gives ∇W at $\mathbf{x}_1$ as

$$W_{x|1} = \frac{1}{2V_{412}} [W_1\,\delta y_{24} + W_2\,\delta y_{41} + W_4\,\delta y_{12}] \tag{A.7a}$$

$$W_{y|1} = -\frac{1}{2V_{412}} [W_1\,\delta x_{24} + W_2\,\delta x_{41} + W_4\,\delta x_{12}], \tag{A.7b}$$

where V_{412} is the area of triangle $(\mathbf{x}_4, \mathbf{x}_1, \mathbf{x}_2)$; note that taking the area-weighted average of four such expressions gives exactly (2.11).

APPENDIX B: FOURIER ANALYSIS OF STABILITY

Strictly speaking, to show convergence of an iterative scheme one must show that all error modes are damped. However, the cell vertex discretisation is known to contain spurious modes which are only damped by the boundary conditions. So for the Fourier analysis we seek only conditions for no error growth: these conditions are then exactly those for so-called practical stability in the unsteady problem. We consider two scalar problems below.

(i) *Convection-Diffusion in One Dimension*

Consider the linear scalar problem

$$w_t + a w_x - \varepsilon w_{xx} = 0, \tag{B.1}$$

where a and ε are nonnegative constants and a uniform mesh spacing h is used. Then the iteration (3.5) reduces to the following approximation to the unsteady problem:

$$W_j^{n+1} = W_j^n - \tfrac{1}{2}\Delta t(D_{j-1/2,j}R_{j-1/2}^n + D_{j+1/2,j}R_{j+1/2}^n). \tag{B.2}$$

Introducing the difference operator $\delta W_{j-1/2} := W_j - W_{j-1}$ and the averaging operator $\sigma W_{j-1/2} := \frac{1}{2}(W_j + W_{j-1})$, we can write the cell residuals as

$$R_{j-1/2}^n = [(a/h)\,\delta - (\varepsilon/h^2)\,\sigma\,\delta^2]\,W_{j-1/2}^n; \tag{B.3}$$

and the distribution matrices, in terms of the cell CFL number v_C, are the scalar quantities

$$D_{j-1/2,j} = 1 + v_C, \qquad D_{j+1/2,j} = 1 - v_C. \tag{B.4}$$

With the notation

$$v_N = a\,\Delta t/h, \qquad \mu_N = \varepsilon\,\Delta t/h^2 \tag{B.5}$$

for the usual dimensionless mesh parameters in a convection-diffusion problem, the iteration (B.2) reduces to

$$W_j^{n+1} = [1 - (\sigma - \tfrac{1}{2}v_C\,\delta)(v_N\,\delta - \mu_N\sigma\,\delta^2)]\,W_j^n, \tag{B.6}$$

the stability of which we will study by Fourier analysis. It should be noted that we have reverted to a standard usage for the CFL numbers v_N or v_C here; this is because the introduction of maximal local time-steps as in the main text is unnecessary for a uniform mesh, and a global time-step is required for the unsteady problem.

Making the usual substitution $W_j^n = \lambda^n e^{ij\xi}\hat{W}$ with $\xi = kh$ and using the abbreviations $s = \sin\frac{1}{2}\xi$, $c = \cos\frac{1}{2}\xi$, we obtain the expression for the amplification factor from (B.6)

$$\lambda(\xi) = 1 - (c - iv_C s)(2iv_N s + 4\mu_N c s^2) \tag{B.7}$$

which gives

$$|\lambda(\xi)|^2 = [1 - 2v_N v_C s^2 - 4\mu_N s^2 c^2]^2 + [2sc(v_N - 2\mu_N v_C s^2)]^2. \tag{B.8}$$

For practical stability we require $|\lambda(\xi)|^2 \leqslant 1$, $\forall\xi$. Necessary conditions result from special cases: setting $s^2 = 1$, $c^2 = 0$ gives $(1 - 2v_N v_C)^2 \leqslant 1$, that is, $v_N v_C \leqslant 1$; and letting $s^2 \to 0$ gives from the coefficient of s^2 the condition $4v_N v_C + 8\mu_N \geqslant 4v_N^2$. We summarise these in the following statement which generalises (3.6):

Necessary stability conditions:

$$v_N v_C \leqslant 1, \qquad v_N^2 \leqslant v_N v_C + 2\mu_N. \tag{B.9}$$

To obtain sufficient conditions, we expand (B.8) and gather terms involving μ_N to obtain after a little manipulation

$$|\lambda|^2 = 1 - 4s^2\{2\mu_N c^2[1 - 2\mu_N s^2 + 2\mu_N(1 - v_C^2)\,s^4] + [v_N v_C(1 - v_N v_C)\,s^2 + v_N(v_C - v_N)\,c^2]\}. \tag{B.10}$$

It is clear that when $\mu_N = 0$, the conditions of (3.6), namely $v_N \leqslant v_C$ and $v_N v_C \leqslant 1$, are sufficient to ensure $|\lambda|^2 \leqslant 1$. Furthermore, it is clear that for $\mu_N > 0$ we require only

$$1 - 2\mu_N s^2 + 2\mu_N(1 - v_C^2)\,s^4 \geqslant 0 \qquad \forall s^2 \in [0, 1]. \tag{B.11}$$

When $v_C^2 \leqslant \frac{1}{2}$, the minimum is attained for $s^2 = \frac{1}{2}(1 - v_C^2)^{-1}$ and equals $1 - \frac{1}{2}\mu_N(1 - v_C^2)^{-1}$; and when $v_C^2 \geqslant \frac{1}{2}$ the minimum of $1 - 2\mu_N v_C^2$ is attained at $s^2 = 1$. We therefore have

Sufficient stability conditions:

$$v_N v_C \leqslant 1, \; v_N \leqslant v_C \tag{B.12a}$$

and

$$\begin{aligned} v_C^2 + \tfrac{1}{2}\mu_N &\leqslant 1 \quad \text{if} \quad v_C^2 \leqslant \tfrac{1}{2} \\ 2\mu_N v_C^2 &\leqslant 1 \quad \text{if} \quad v_C^2 \geqslant \tfrac{1}{2}. \end{aligned} \tag{B.12b}$$

This region is plotted in Fig. 11 for the special case $v_N = v_C$. Also plotted is the stability region for the standard Lax–Wendroff scheme for the convection-diffusion equation which is just $v^2 + 2\mu \leqslant 1$. Note that the cell-vertex conditions are not only much less stringent but that the condition $v^2 = 1$ is stable right up to $\mu = \frac{1}{2}$. Thus in the main text above (3.3a), we have based the choice of time-step on ensuring both $v^2 \leqslant 1$ and $\mu \leqslant \frac{1}{2}$.

(ii) *Convection in Two Dimensions*

We consider the equation

$$w_t + aw_x + bw_y = 0, \tag{B.13}$$

where a and b are nonnegative constants; also there is no loss of generality in assuming a square mesh and $b \leqslant a$. The cell residuals have the form, using subscripts to denote the difference operators in the x and y directions,

$$R = [(a/h)\,\delta_x\sigma_y + (b/h)\,\delta_y\sigma_x]\,W, \tag{B.14}$$

and the distribution matrices have the form

$$D = 1 \pm v_{Cx} \pm v_{Cy}. \tag{B.15}$$

With the notation

$$v_{Nx} = a\,\Delta t/h, \qquad v_{Ny} = b\,\Delta t/h, \tag{B.16}$$

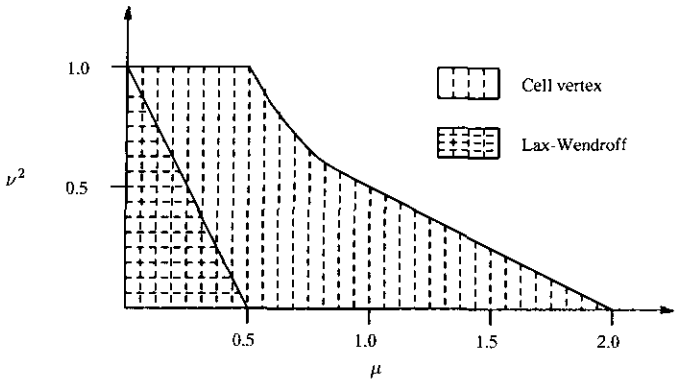

FIG. 11. Stability regions of the cell vertex method and the conventional Lax–Wendroff method.

the iteration becomes

$$W_j^{n+1} = [1 - (\sigma_x - \tfrac{1}{2}\nu_{Cx}\delta_x)(\sigma_y - \tfrac{1}{2}\nu_{Cy}\delta_y) \times (\nu_{Nx}\delta_x\sigma_y + \nu_{Ny}\delta_y\sigma_x)]\, W_j^n. \quad \text{(B.17)}$$

Writing $m_N = \nu_{Nx}s_xc_y + \nu_{Ny}s_yc_x$, where $s_x = \sin\frac{1}{2}\xi = \sin\frac{1}{2}k_xh$ etc., and similarly for m_C, the amplification factor is easily seen to be

$$\lambda(\xi, \eta) = 1 - 2im_N(c_xc_y - im_C) \quad \text{(B.18)}$$

which gives

$$|\lambda|^2 = (1 - 2m_Nm_C)^2 + 4m_N^2c_x^2c_y^2 = 1 - 4m_N[m_C - m_Nc_x^2c_y^2 - m_Nm_C^2]. \quad \text{(B.19)}$$

It is clear that as $s_x, s_y \to 0$ it is necessary that $m_C \geqslant m_N$ for all values of the ratio $s_x : s_y$, giving

Necessary stability conditions:

$$\nu_{Cx} : \nu_{Cy} = \nu_{Nx} : \nu_{Ny} = a/b \quad \text{(B.20a)}$$

and

$$\nu_C^2 := \nu_{Cx}^2 + \nu_{Cy}^2 \geqslant \nu_{Nx}^2 + \nu_{Ny}^2 =: \nu_N^2. \quad \text{(B.20b)}$$

The sufficient conditions are quite complicated and need some further notation: we write

$$\alpha^2 := 1 - \nu_N/\nu_C, \qquad \tan\psi := b/a, \qquad \hat{\nu}^2 := \nu_N\nu_C. \quad \text{(B.21)}$$

Then writing $t_x = s_x/c_x = t\cos(\theta + \psi)$, $t_y = s_y/c_y = t\sin(\theta + \psi)$, we have

$$m_N = \nu_Nc_xc_y(t_x\cos\psi + t_y\sin\psi) = \nu_Ntc_xc_y\cos\theta = \nu_Nm_C/\nu_C. \quad \text{(B.22)}$$

Hence (B.19) reduces to

$$|\lambda|^2 = 1 - 4m_Nm_Cc_x^2c_y^2[(1 + t_x^2)(1 + t_y^2) - (\nu_N/\nu_C) - \hat{\nu}^2t^2\cos^2\theta] \quad \text{(B.23)}$$

and the stability condition becomes

$$\hat{\nu}^2 \leqslant \min_{t,\theta}\left\{\frac{\alpha^2t^{-2} + 1 + \frac{1}{4}t^2(\sin 2(\theta + \psi))^2}{\cos^2\theta}\right\}. \quad \text{(B.24)}$$

The minimum with respect to t^2 occurs at $t^2 = 2\alpha/\sin 2(\theta + \psi)$, so we have

$$\hat{\nu}^2 \leqslant \min_{\theta}\left\{\frac{1 + \alpha\,|\sin 2(\theta + \psi)|}{\cos^2\theta}\right\}. \quad \text{(B.25)}$$

Further manipulation results in the stability region shown in Fig. 12, where we have also shown the case $b \geqslant a$ using symmetry. In the standard Lax–Wendroff case, $\alpha = 0$, we have just $\hat{\nu}^2 \leqslant 1$ as is well known; but more generally we have, together with (B.20),

Necessary and sufficient conditions:

$$\hat{\nu}^2 \leqslant 1 + \alpha\left(\frac{\sin 2\psi - \alpha}{1 - \alpha\sin 2\psi}\right) \quad \text{if} \quad \alpha \leqslant \tan\psi \quad \text{(B.26a)}$$

$$\hat{\nu}_x = \hat{\nu}\cos\psi \leqslant 1 \quad \text{if} \quad \alpha \geqslant \tan\psi. \quad \text{(B.26b)}$$

Thus as ν_C is increased relative to ν_N, the stability region expands from the quarter-circle to the whole square, $0 \leqslant \nu_x, \nu_y \leqslant 1$.

Finally, one can combine the results for the two problems (B.1) and (B.13) to cover two-dimensional convection-diffusion. We have seen in (B.12) that the key advantage in treating the convective and diffusive fluxes consistently

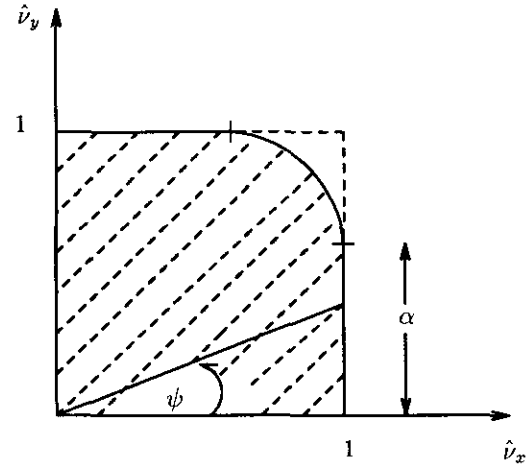

FIG. 12. Stability region for the generalised Lax–Wendroff method (2D convection).

shows itself for $v_C = v_N$. In that case, it is shown in [14] that a sufficient stability condition in the 2D case is

$$v_x^2 + v_y^2 \leqslant 1 \qquad \text{and} \qquad \mu_x + \mu_y \leqslant \tfrac{1}{2}, \qquad \text{(B.27)}$$

in an obvious notation.

6. ACKNOWLEDGMENTS

The authors would like to thank British Aerospace (Military Aircraft) Ltd. for funding and CRAY time. The second author also gratefully acknowledges financial support from the Science and Engineering Research Council.

REFERENCES

1. B. S. Baldwin and H. Lomax, AIAA Paper 78-257, 1978 (unpublished).
2. F. Casier, H. Deconinck, and Ch. Hirsch, *AIAA J.* **22**, 1556 (1984).
3. P. H. Cook, M. A. McDonald, and M. C. P. Firmin, AGARD-AR-138, 1979 (unpublished).
4. P. I. Crumpton, J. A. Mackenzie, K. W. Morton, M. A. Rudgyard, and G. J. Shaw, in *Twelfth International Conference on Numerical Methods in Fluid Dynamics. Proceedings, Conference, University of Oxford, England July 1990*, Lecture Notes in Physics, Vol. 371, edited by K. W. Morton (Springer-Verlag, New York/Berlin, 1990), p. 243.
5. E. Dick, *J. Comput. Phys.* **76**, 19 (1988).
6. K. P. Dimitriadis and M. A. Leschziner, in *Proceedings, Fourth Copper Mountain Conference on Multigrid Methods* (SIAM, Philadelphia, 1989), p. 130.
7. B. Garcia-Archilla and J. A. Mackenzie, Technical Report NA91/13, Oxford University Computing Laboratory, 1991 (unpublished).
8. V. A. Gushchin and V. V. Shchennikov, *U.S.S.R. Comput. Math. Math. Phys.* **14**, 252 (1974).
9. M. G. Hall, in *Proceedings, Conference on Numerical Methods for Fluid Dynamics, University of Reading*, edited by K. W. Morton and M. J. Baines (Oxford University Press, London, 1985), p. 303.
10. M. G. Hall, AIAA Paper 91-1540, 1991 (unpublished).
11. A. Jameson, W. Schmidt, and E. Turkel, AIAA Paper 81-1259, 1981 (unpublished).
12. J. E. Lavery, *J. Comput. Phys.* **79**, 436 (1988).
13. J. E. Lavery, *J. Comput. Phys.* **86**, 1 (1990).
14. J. A. Mackenzie, Ph.D. thesis, Oxford University Computing Laboratory, 1991 (unpublished).
15. J. A. Mackenzie and K. W. Morton, *Math. Comput.* **60**, 189 (1992).
16. L. Martinelli, Ph.D. thesis, Dept. of Mech. and Aerospace Eng., Princeton University, 1987 (unpublished).
17. D. J. Mavriplis, A. Jameson, and L. Martinelli, AIAA Paper 89-0120, 1989 (unpublished).
18. K. W. Morton, in *The Mathematics of Finite Elements and Applications VI, MAFELAP 1987*, edited by J. R. Whiteman (Academic Press, New York/London, 1988), p. 353.
19. K. W. Morton, P. N. Childs, and M. A. Rudyard, Technical Report NA88/5, Oxford University Computing Laboratory, 1988 (unpublished).
20. K. W. Morton, P. I. Crumpton, and J. A. Mackenzie, *Comput. & Fluids* **22**, No. 2/3, 91 (1993).
21. K. W. Morton and M. F. Paisley, *J. Comput. Phys.* **80**, 168 (1989).
22. K. W. Morton and M. A. Rudgyard, Technical Report NA89/11, Oxford University Computing Laboratory, 1989; in *Proceedings of GAMNI/SMAI–IMA Conference on Computational Aeronautical Fluid Dynamics, Antibes 1989* (unpublished).
23. K. W. Morton, M. A. Rudgyard, and G. J. Shaw, Technical Report NA91/09, Oxford University Computing Laboratory, 1991 (unpublished).
24. R. H. Ni, *AIAA J.* **20**, 1565 (1982).
25. T. H. Pulliam and J. L. Steger, AIAA Paper 86-0274, 1986 (unpublished).
26. R. Radespiel and C. Rossow, DFVLR-IB 129-87/40, 1987 (unpublished).
27. R. Radespiel and R. C. Swanson, AIAA Paper 89-0548, 1989 (unpublished).
28. E. Süli, Technical Report NA89/6, Oxford University Computing Laboratory, 1989 (unpublished).
29. R. C. Swanson and E. Turkel, AIAA Paper 85-0035, 1985 (unpublished).
30. R. C. Swanson and E. Turkel, ICASE Report 90-44, NASA, 1990 (unpublished).
31. J. L. Thomas and M. D. Salas, *AIAA J.* **24**, 1074 (1986).